Experimental Research

INTERNATIONAL JOURNAL OF SURGERY

OPEN

LINC00476 cooperates with ARIH2 and suppresses pancreatic cancer progression by inducing VIM ubiquitination

Qian Yan, PhD[a], Yubin Chen, MSc[a,b], Zhenchong Li, MSc[a,b,c], Shiye Ruan, MD[a], Zhongyan Zhang, MSc[a], Jinwei Cui, MSc[a], Hexian Shi, MSc[a], Jike Fang, MSc[a], Hailiang Wang, MSc[a], Jiayu Yang, MSc[a], Shanzhou Huang, PhD[a,*], Chuanzhao Zhang, PhD[a,*], Baohua Hou, PhD[d,e,f,*]

Background: Pancreatic ductal adenocarcinoma (PDAC) remains one of the deadliest solid malignancies, with the majority of cases typically diagnosed at an advanced, inoperable stage. Dysregulated long noncoding RNAs (lncRNAs) play a significant role in the progression of PDAC; however, the underlying mechanisms, especially the interactions between lncRNAs and protein modifications, remain poorly understood.

Method: We initially screened for potential markers among pancreatic cancer-associated lncRNAs using public databases. The involvement of LINC00476 in PDAC cell proliferation, migration, and invasion was confirmed through both *in vivo* and *in vitro* experiments. To dissect the molecular mechanisms underlying LINC00476-mediated regulation of PDAC progression and metastasis, we utilized RNA pull-down assays, RNA immunoprecipitation (RIP) assays, Co-immunoprecipitation (Co-IP) assays, and rescue experiments.

Result: Our findings identify LINC00476 as a novel lncRNA that is generally downregulated in PDAC tissues and correlates with more unfavorable clinicopathological features and poorer patient outcomes. Functionally, LINC00476 suppressed PDAC cell proliferation and invasion *in vitro* and inhibited lung metastasis *in vivo*. Mechanistically, LINC00476 directly bound vimentin (VIM) and recruited the E3 ubiquitin ligase Ariadne homolog 2 (ARIH2), promoting K29-linked polyubiquitination of VIM at Lys373 residue and subsequent proteasomal degradation. In a patient-derived xenograft (PDX) model, overexpression of ARIH2 led to a significant reduction in VIM protein levels and tumor growth ($P < 0.05$).

Conclusion: Our data suggest that LINC00476 enhances VIM ubiquitination and degradation by recruiting ARIH2, highlighting the role of LINC00476 in PDAC progression and indicating that the overexpression of LINC00476 or ARIH2 may serve as a promising therapeutic strategy for PDAC.

Keywords: ARIH2, LINC00476, pancreatic ductal adenocarcinoma (PDAC), ubiquitination (Ub), vimentin (VIM)

Introduction

Pancreatic ductal adenocarcinoma (PDAC) is the third leading cause of cancer-related deaths with a low overall survival rate of 5 years[1,2]. The lack of a reliable test for early diagnosis and limited efficacy of available treatments for advanced PDAC mainly account for the poor prognosis[3]. Thus, it is critical to understand the molecular mechanism underlying PDAC development and identifying novel biomarkers for improving patient care.

Long noncoding RNAs (lncRNAs) offer a novel perspective on understanding complex biological functions, characterized by transcripts longer than 200 nucleotides that possess little or no protein-coding capacity[4]. By interacting with miRNAs, mRNAs, DNAs, or proteins, lncRNAs play significant roles in various aspects of cellular homeostasis in cancers, including proliferation, survival, migration, and genomic stability[5–8]. Increasing evidence underscores the critical roles of lncRNAs in the tumorigenesis and metastasis of PDAC. For instance, we previously demonstrated that LINC00909 regulates SMAD4 expression at the posttranscriptional level, promoting cancer stemness and metastasis in PDAC[9]. Epithelial-to-mesenchymal transition (EMT) confers

[a]Department of General Surgery, Guangdong Provincial People's Hospital (Guangdong Academy of Medical Sciences), Southern Medical University, Guangzhou, China, [b]Department of Medicine II, University Medical Center Mannheim, Medical Faculty Mannheim, Heidelberg University, Mannheim, Germany, [c]Junior Clinical Cooperation Unit Translational Gastrointestinal Oncology and Preclinical Models, German Cancer Research Center (DKFZ), Heidelberg, Germany, [d]Department of General Surgery, Heyuan People's Hospital, Heyuan, China, [e]Heyuan Key Laboratory of Molecular Diagnosis & Disease Prevention and Treatment, Heyuan People's Hospital, Heyuan, China and [f]Department of General Surgery, Maoming People's Hospital, Maoming, China

Qian Yan, Yubin Chen, and Zhenchong Li contributed equally to this work.

Sponsorships or competing interests that may be relevant to the content are disclosed at the end of this article.

*Corresponding authors. Address: Department of General Surgery, Guangdong Provincial People's Hospital (Guangdong Academy of Medical Sciences), Southern Medical University, Guangzhou 510080, China. Tel.: +8613928842869. E-mail: hshanzh@163.com (S. Huang); Tel.: +8615102099746. E-mail: zhangchuanzhao@gpdh.org.cn (C. Zhang); Heyuan People's Hospital, Heyuan 517000, China. Tel.: +8613609006510. E-mail: hbh1000@126.com (B. Hou).

International Journal of Surgery (2026) 112:666–682

Received 6 January 2025; Accepted 23 September 2025

Supplemental Digital Content is available for this article. Direct URL citations are provided in the HTML and PDF versions of this article on the journal's website, www.lww.com/international-journal-of-surgery.

Published online 7 October 2025

http://dx.doi.org/10.1097/JS9.0000000000003596

cells with the ability to metastasize and invade. It is characterized by stem cell-like properties, reduced apoptosis and senescence, and enhanced immunosuppression. EMT plays a crucial role not only in development but also in processes such as tissue healing, organ fibrosis, and carcinogenesis. NORAD has been reported to induce EMT to facilitate invasion and metastasis as a competing endogenous RNA[10]. In addition, SLC7A11-AS1 can scavenge reactive oxygen species (ROS), thereby conferring resistance to Gemcitabine by inhibiting SCFβ-TRCP-mediated ubiquitination and degradation of NRF2[11].

Vimentin (VIM), a type III intermediate filament protein, is highly expressed in aggressive epithelial cancers, including lung and gastric cancers, and plays a crucial role in cancer progression[12–14]. In particular, epithelial cancer cells exhibiting VIM overexpression may undergo EMT, ultimately leading to metastasis. Aberrant expression of VIM is prominent in PDAC cells, contributing to a mesenchymal phenotype that enhances the invasive potential of these cells. VIM regulates cell adhesion and motility via phosphorylation (soluble form) and dephosphorylation (insoluble form)[15,16]. Furthermore, posttranslational modifications (PTMs), such as *O*-linked glycosylation, ubiquitination, sumoylation, and acetylation, are known to modulate the function of VIM[17]. Recently, the E3 ubiquitin ligase, TRIM56, has been identified as a negative regulator of VIM, promoting polyubiquitination-mediated proteasomal degradation, which results in decreased cell migration and invasion[18]. Although the function of VIM in cancer metastasis has been extensively studied, the interaction between lncRNAs and VIM remains unclear, as does the mechanism by which lncRNAs regulate the PTM of VIM. In this study, we profiled the differential expression of lncRNAs between patients with PDAC and healthy individuals. We found that LINC00476 was significantly downregulated in patients with PDAC, and its expression was positively associated with patient survival. Notably, LINC00476 has previously been described as a tumor suppressor in lung cancer[19]. Through *in vitro* and *in vivo* experiments, we demonstrated that LINC00476 inhibits pancreatic cancer cell invasion and suppresses tumor growth and metastasis. Moreover, LINC00476 interacts with VIM and promotes its ubiquitination by Ariadne homolog 2 (ARIH2), a key member of the RING-between-RING (RBR) E3 ligase family. Thus, we identified LINC00476 as a novel tumor suppressor in PDAC.

HIGHLIGHTS

- LINC00476 downregulates vimentin (VIM) and inhibits the epithelial-to-mesenchymal transition (EMT) process.
- LINC00476 cooperates with the E3 ubiquitin ligase Ariadne homolog 2 (ARIH2) to induce VIM ubiquitination.
- LINC00476 is associated with more unfavorable clini copathologic features and poorer outcomes.
- LINC00476 binds to VIM, promoting the ubiquitination dependent degradation by recruiting the ubiquitinase ARIH2.

Methods and materials

Cell lines, drugs, reagents, and antibodies

PDAC cell lines (AsPC-1 and MIA PaCa-2) and human embryonic kidney cells (HEK-293T) were acquired from the Cell Bank of the Chinese Academy of Sciences (Shanghai, China). AsPC-1 cells were cultured in RPMI 1640 medium (Gibco), whereas MIA PaCa-2 and HEK-293T cells were maintained in high-glucose DMEM (Gibco). All media were supplemented with 10% fetal bovine serum (FBS; Gibco), along with 100 IU/mL penicillin and 100 μg/mL streptomycin (NCM, Suzhou, China). Cells were cultured at 37°C in a humidified atmosphere containing 5% CO_2. All cell lines were authenticated using STR profiling and tested for mycoplasma contamination. MG132 and CHX were procured from Sigma (Shanghai, China). Antibodies including anti-VIM, anti-ARIH2, anti-E-cadherin, anti-N-cadherin, anti-MMP9, anti-Ub, anti-GAPDH, anti-HA, anti-His, and anti-Flag were purchased from Proteintech (Wuhan, China), while the anti-PCNA antibody was obtained from BD Biosciences. All antibodies were diluted in accordance with the manufacturer's instructions.

Patients and clinical samples

Sixty pairs of primary PDAC specimens were collected from patients who underwent surgical resection of pancreatic cancer between February 2010 and June 2023. All PDAC tissue samples were stored at a temperature of –80°C after collection. A summary of the clinicopathological characteristics of the patients is presented in Table 1. This study was approved by the Ethics Committee.

Transfection and infection experiments and plasmids

Small-hairpin shRNAs targeting ARIH2 and VIM, along with a negative control shRNA (sh-NC), were obtained from Gene Pharma Co. Ltd. (Shanghai, China) and transfected using the lipofectamine 2000 Transfection Kit (Invitrogen, Carlsbad, CA, USA). The knockout of LINC00476 in MIA PaCa-2 PDAC cells, which were at log phase, was performed using a custom-made Cas9-sgRNA LINC00476 knockout kit (GeneCopoeia), adhering to the manufacturer's instructions. Briefly, vectors containing the Cas9 gene and sgRNA designed to target the promoter sequence of LINC00476 were transfected into MIA PaCa-2 cells (designated as Mia-NC for the negative control, and KO3 and KO6 for the knockout of LINC00476). Following transfection, single-cell clones were isolated through serial dilutions. The selection of LINC00476 knockout clones was conducted using the IndelCheck™ kit provided with the knockout kit, in accordance with the manufacturer's guidelines. For the overexpression system, the dCAS9-SAM approach was employed, with LV serving as the control for LINC00476 overexpression. Lentiviruses were produced in HEK-293T cells by cotransfecting the targeting plasmids along with the packaging plasmid psPAX2 and the envelope plasmid pMD2.G. After 48 h, viral supernatants were collected and filtered through 0.45 μm-diameter pore filters (Millipore, USA). The ubiquitination plasmid containing an HA tag was procured from RiboBio (Guangzhou, China). Recombinant plasmids containing full-length human ARIH2 and VIM cDNA cloned into the PCDH-CMV-MCS-EF1-Hygro vector, with the His tag and Flag tag sourced from RiboBio (Guangzhou, China). In addition, the ubiquitin mutant plasmids (K27R, K29R, K48R, and K63R) featuring the HA tag, the ARIH2 mutant plasmid (C317A) with the His tag, and the VIM mutant plasmid (K373R) with the Flag tag were also obtained from RiboBio

Table 1

Clinicopathological characteristics of 60 patients with PDAC in the GDPH cohort

	LINC00476		
Characteristics	**Low**	**High**	***P* value**
Sex			0.793
Female	18	17	
Male	12	13	
Age (years)			0.436
≥60	12	15	
<60	18	15	
AJCC stage			**0.004**
III/IV	19	8	
I/II	11	22	
Lymph nodes			**0.004**
Positive	18	7	
Negative	12	23	
Differentiation			**0.010**
Poor	19	9	
Well	11	21	

AJCC, American Joint Committee on Cancer.
The chi-square test was used and *P* values less than 0.05 were considered statistically significant.

(Guangzhou, China). In the transfection and infection experiments, target plasmids and packaging plasmids were transfected into HEK-293T cells using the transfection reagent Lipofectamine 2000 (Invitrogen, Carlsbad, CA, USA). Lentiviruses were harvested 48 h later and utilized to infect PDAC cells twice, with each infection lasting 24 h. The infected cells were subsequently screened through treatment with puromycin for 36 h, and the surviving cells were frozen and stored in liquid nitrogen for future experiments. All primers for the shRNA sequences are provided in Supplemental Digital Content Table S1, available at: http://links.lww.com/JS9/F273.

Proliferation

The CCK-8 assay was conducted to assess cell viability, utilizing the CCK-8 reagent obtained from Beyotime (Shanghai, People's Republic of China) in accordance with the manufacturer's instructions. The optical density at 450 nm (OD450) of each cell culture, following the addition of the CCK-8 reagent, was measured at various time points using a microplate reader. For the colony formation assays, PDAC cells were seeded into six-well plates at a density of 3000 cells per well. These cells were incubated at 37°C in a 5% CO_2 atmosphere for a duration of 7 days. After rinsing with phosphate-buffered saline (PBS), the cells were stained with 0.1% crystal violet to facilitate the observation of colony formation.

Wound-healing and Transwell assays

When the cell density in the six-well plate reached 85%, we utilized a sterile pipette tip to create a scratch in the center of each well. Wound healing was assessed at 0 and 24 h, with the size of the wound measured at least three times. For Transwell assays, a total of 5×10^3 PDAC cells were seeded in the upper chamber of Transwell plates containing the DMEM supplemented with 5% FBS, while 800 μL of DMEM containing 20% FBS was added to the lower chamber. Following incubation at 37°C for 24–48 h, the cells migrated from the upper chamber to the lower chamber. The upper chambers were then removed and washed three times with PBS, after which the cells were fixed with 4% paraformaldehyde (G1101; Servicebio, Wuhan, China) and stained with 0.1% crystal violet (C0121; Beyotime, Beijing, China). Transwell membranes coated with matrix were employed for invasion experiments, whereas those used for migration experiments were left uncoated. The number of PDAC cells was quantified using a microscope (Olympus, Tokyo, Japan).

Immunohistochemistry staining and in situ *hybridization*

Paraffin-embedded tumors were dewaxed and hydrated and then immersed in citrate buffer (pH 6.0) and heated in a microwave oven to 95°C for 20 min. Following this, the endogenous peroxidase activity was quenched, and blocking was performed using normal goat serum. Antibodies were diluted with BSA according to the manufacturer's instructions and were added to the paraffin sections, where they were incubated overnight at 4°C. Afterward, a horseradish peroxidase-linked secondary antibody was applied and incubated with the sections, followed by the addition of 3,3′-diaminobenzidine (DAB). *In situ* hybridization was conducted using a PDAC and normal tissue micro-array and utilized for detecting LINC00476 expression in tissue using specific 5′- and 3′-digoxigenin-labeled probes. The slides were dewaxed twice in xylene (5 min each), then dehydrated via a graded ethanol series: 100% ethanol (2 min), 95% ethanol (2 min), 80% ethanol (2 min). After air-drying, the plates were incubated with hydrogen peroxide for 10 min and then rinsed five times with distilled water. They were then treated with Proteinase K and incubated at 40°C for 5 h in Hybridisation Reagent containing probes (1042471-C1, Advanced Cell Diagnostics). After being washed, the sections were incubated with DAB, and counterstaining was carried out using hematoxylin. The results were examined under a microscope prior to counterstaining with DAB, and then quantified according to the intensity of staining (0 = negative, 1 = weak, 2 = moderate, and 3 = strong) and the extent of staining (1 = 0–25%, 2 = 26–50%, 3 = 51–75%, and 4 = 76–100%). A risk score was derived by multiplying the percentage of positive cells with staining intensity divided by 10.

Fluorescence in situ *hybridization and immunofuorescence staining*

The fluorescence *in situ* hybridization (FISH) probes used in this study were designed and synthesized by RiboBio (Guangzhou, China). FISH assays and immunofuorescence (IF) staining were performed according to a previously described method[20]. Briefly, for FISH, after counter staining with DAPI (Beyotime, Shanghai, China), slides were visualized under a Leica SP8 X confocal microscope (Leica, Germany). IF staining was performed using an anti-VIM antibody (1:250 dilution, 0366-1-AP, Proteintech) and an anti-ARIH2 antibody (1:250 dilution, 15006-1-AP, Proteintech).

Western blot

RIPA buffer was employed for cell lysis to extract proteins from the cells, followed by denaturation and separation of the proteins. Proteins of varying molecular weights were resolved

using SDS-polyacrylamide gel electrophoresis and subsequently electrotransferred to polyvinylidene difluoride (PVDF) membranes. The membranes were blocked with skimmed milk for the detection of total proteins and with BSA for the detection of phosphorylated proteins. Membrane sections were incubated sequentially with primary antibodies, followed by secondary antibodies. The membranes were then exposed to ECL Reagent (Cell Signaling) and visualized using a Western blot detection system (Thermo Fisher, Shanghai, China). The specific antibodies utilized in this study are detailed in Supplemental Digital Content Table S2, available at: http://links.lww.com/JS9/F274. Three independent experiments were conducted.

Quantitative and reverse transcription PCR

Total RNA was extracted from cells using TRIzol reagent (Invitrogen, California, USA. Subsequently, 2 μg of RNA was reverse transcribed into complementary DNA (cDNA). The normalized expression control was based on the glyceraldehyde-3-phosphate dehydrogenase (GAPDH) value. Finally, mRNA expression was quantified as the cycle threshold (CT) value. All quantitative primers are listed in the Supplemental Digital Content Table S3, available at: http://links.lww.com/JS9/F275.

Immunoprecipitation

Initially, cells were transfected with a specific plasmid, and the transfected cells were subsequently lysed in an immunoprecipitation (IP) lysis buffer solution (HY-K1002, MCE, USA). Following this, proteins were extracted from the cells. The target protein was then incubated overnight at 4°C with a defined proportion of primary antibody. Subsequently, 50 μL of protein A + G agarose beads (HY-K0202, MCE, USA) was added to the protein-antibody mixture and incubated at 4°C for 4 h. After incubation, the target proteins were bound to the beads, which were then washed with precooled PBS to eliminate impurities. The protein samples were then combined with 40 μL of an 1× loading buffer solution and heat-denatured. After these steps, the protein samples were separated using SDS-polyacrylamide gel electrophoresis and electrotransferred to PVDF membranes. The membranes were incubated with primary antibodies overnight at 4°C, followed by a 2-h incubation with secondary antibodies. Finally, the membranes were exposed and analyzed using a Chemiscope 6000 imaging system.

RNA pull down

Initially, cells were transfected with a specific plasmid. Subsequently, a magnetic RNA pull-down kit (20164, Pierce) was employed for LINC00476 pull-down assays. Biotinylated RNA was transcribed using Biotin RNA Labeling Mix and T7 RNA polymerase. The purified biotinylated RNA was then heated and annealed to achieve the appropriate secondary structure before being incubated with PDAC cell lysates for 1 h at 4°C. Following this, the mixture was combined with streptavidin–agarose beads (Invitrogen) and incubated for an additional hour at room temperature. Finally, the enriched proteins were separated by SDS–PAGE for subsequent analysis via mass spectrometry or Western blotting.

RNA immunoprecipitation assay

An EZ-Magna RNA immunoprecipitation (RIP) Kit (Millipore) was utilized to conduct the RIP assay in accordance with the manufacturer's protocol. Approximately 1×10^7 MIA PaCa-2 or AsPC-1 cells were harvested and lysed using a 100% RIP lysis buffer solution supplemented with proteinase and RNase inhibitors. The RIP lysates were subsequently incubated with the RIP buffer solution containing magnetic beads conjugated to an anti-VIM (ab194297, Abcam) antibody, an anti-ARIH2 antibody (15006-1-AP, Proteintech), an anti-Flag antibody (14793S, CST, Danvers, USA), or control IgG (Millipore). The enrichment of LINC00476 was assessed using qRT–PCR.

Cell fractionation

Cell Nuclear and Cytoplasmic fractionation were performed using the Nuclear and Cytoplasmic Protein Extraction Kit (P0028, Beyotime, Beijing, China) according to the manufacturer's instructions. Briefly, 1×10^7 cells were resuspended in 500 μL of a hypotonic buffer solution (10 mM HEPES [pH: 7.9], 10 mM KCl, 1.5 mM $MgCl_2$, and 0.5 mM DTT). The suspension was thoroughly vortexed and agitated for 10–30 min at 4°C. Following centrifugation at 2000*g* for 5 min, the resulting supernatant was collected as the cytoplasmic fraction. The obtained pellet was then resuspended in an S1 buffer solution (0.25 M sucrose and 10 mM $MgCl_2$), layered onto 300 μL of an S2 buffer solution (0.35 M sucrose and 0.5 mM $MgCl_2$), and subjected to centrifugation at 1500*g* for another 5 min. The pellet was resuspended in the S2 buffer solution to serve as the nuclear fraction. The nuclear fraction underwent sonication for 2 s, followed by 3-s intervals over a span of 6–7 min, before being overlaid onto an S3 buffer solution (0.88 M sucrose, 0.05 mM $MgCl_2$). Centrifugation at approximately 3000*g* for 10 min allowed for the collection of the resulting supernatant as the nucleoplasmic fraction, while the obtained pellet was resuspended in the RIPA buffer solution to serve as the nucleolar fraction. The fractions were subsequently resolved through an SDS-PAGE analysis followed by immunoblotting or qRT-PCR.

Ubiquitination assay

For the *in vivo* ubiquitination assay, cells were co-transfected with the specified plasmids. After 48 h of transfection, the cells were treated with 10 μM of the proteasome inhibitor MG132 (S2619, Selleckchem, USA) for 6 h. Subsequently, the cells were lysed in Cell Lysis Buffer (Sigma) for Western blotting and IP, following the same protocol utilized for co-immunoprecipitation (Co-IP).

Turnover assay

The cells were transfected with the specified plasmids. Cycloheximide (CHX) (HY-12320, MCE) was added to the media at a final concentration of 50 μg/ml. The cells were harvested at the designated time points following CHX treatment. Protein levels were assessed using a Western blot assay.

In vivo functional assays

The subcutaneous xenograft mice model was established to evaluate tumor formation *in vivo*. The *in vivo* metastatic ability was investigated using tail vein and splenic injection experiments.

Animal experiments were approved by the Committee for Animal Protection and Utilization of GDPH. All experiments were conducted in accordance with the Guidelines for Animal Health and Use (Ministry of Science and Technology, China, 2006). For the subcutaneous xenograft assay, MIA PaCa-2 cells (5×10^6 cells/site) were subcutaneously injected into the right flanks of female BALB/c nude mice (4–6 weeks old). Four weeks later, the mice were killed; the tumors were excised and weighed, and the volume was measured (V = length × width^2/2), before placing in 10% neutral-buffered formalin for histological analysis. The *in vivo* metastatic ability was investigated by the splenic injection experiment. For the splenic injection experiment, 5×10^5 cells resuspended in 50 μL of serum-free DMEM were injected into the spleens of the tested nude mice. All of the mice were euthanized 12 weeks post-injection. Tumors formed on the livers were detected macroscopically. Livers were excised from mice, fixed with 4% PFA, and embedded in paraffin; sections of those tissues were used for histological analysis. The study has been reported in accordance with the ARRIVE guidelines (Animals in Research: Reporting In Vivo Experiments)[21].

Patient-derived xenograft mouse model

Four- to five-week-old female nude mice were used for the patient-derived xenograft (PDX) mice experiments. Mice were randomly divided into two groups (Vector, ARIH2-OE). Fresh tumor tissues were cut to pieces with the same weight and then transplanted into the right back of the mice. When the volume of the xenografts reached 200 mm^3, the lentivirus were injected at a dose of 5×10^6 TU/100 μL per mouse, twice a week for 3 weeks. Mice weight and tumor volume were monitored once a week. Thereafter, the mice were anesthetized, and the tumors were weighed. All tumors were extracted for further histological analysis. The work has been reported in accordance with the ARRIVE guidelines (Animals in Research: Reporting In Vivo Experiments)[21].

RNA sequencing and data analysis

High-throughput sequencing of RNA from LINC00476 overexpression PANC-1 cells was conducted by CloudSeq Biotech (Shanghai, China). In brief, rRNA was removed from total RNA using the NEBNext rRNA Depletion Kit (New England Biolabs, Inc., Massachusetts, USA), by following the manufacturer's instructions. RNA libraries were constructed using the NEBNext® Ultra™ II Directional RNA Library Prep Kit (New England Biolabs, Inc., Massachusetts, USA), also in accordance with the manufacturer's guidelines. The quality and quantity of the libraries were assessed using a BioAnalyzer 2100 system (Agilent Technologies, Inc., USA). Library sequencing was performed on an Illumina NovaSeq 6000 instrument, generating 150 bp paired-end reads. The paired-end reads were retrieved from the Illumina NovaSeq 6000 sequencer and underwent quality control using Q30. Following 3′ adaptor trimming and the removal of low-quality reads with Cutadapt software (v1.9.3), the high-quality clean reads were aligned to the reference genome (UCSC hg19) using HISAT2 software (v2.0.4). Subsequently, guided by the Ensembl GTF gene annotation file, the Cuffdiff tool (part of Cufflinks) was employed to derive gene expression data in FPKM, representing the mRNA expression profiles. Fold change and *P*-values were calculated from the FPKM values to identify differentially expressed mRNAs. Gene Ontology (GO) and pathway enrichment analyses were then conducted based on the differentially expressed mRNAs. Details are in Supplemental Digital Content Table S4, available at: http://links.lww.com/JS9/F276.

Mass spectrum analysis

Mass spectrum analysis was conducted according to standard procedures. In brief, the precipitates co-pulled down with RNA using antisense/sense biotin-labeled probes were separated using SDS-PAGE and subsequently stained with silver. The distinct bands were excised and analyzed via matrix-assisted laser desorption/ionization time-of-flight/time-of-flight mass spectrometry. Proteins identifed from the mass spectrometry analysis are listed in Supplemental Digital Content Table S5, available at: http://links.lww.com/JS9/F277.

Bioinformatic analysis of public datasets

Datasets were downloaded from the Gene Expression Omnibus (GEO) database, The Cancer Genome Atlas (TCGA, https://cancergenome.nih.gov/), and the Genotype-Tissue Expression (GTEx) database. Univariable and multivariable Cox proportional regression analyses were conducted to evaluate the association between individual DELnc expression and patients' overall survival (OS) across different batches, utilizing the R packages survival, survminer, and parallel in R version 3.5.2 (https://www.r-project.org/). The Kaplan–Meier method was employed for survival analysis.

Statistical analysis

All experiments were conducted in triplicate, and the statistical parameters, including sample size and significance analysis, are detailed in the figure legends. A two-tailed Student's *t*-test was employed to assess significance at a 95% confidence level, assuming normal distribution with distinct but comparable standard deviations. The quantitative data are presented as the mean ± standard deviation, with a *P*-value of <0.05 considered statistically significant.

Result

LINC00476 is downregulated in PDAC and is associated with patients survival

To identify lncRNAs potentially involved in PDAC, we screened 186 lncRNAs from meta-GEO pancreatic cancer datasets by matching gene symbols from these datasets with the human genome (Ensemble genome browser version 90). Utilizing the R package limma, we identified 61 differentially expressed lncRNAs (DElncRNAs) that met a significance threshold of $P < 0.05$. The expression values of these 61 DElncRNAs were subsequently extracted from The Cancer Genome Atlas (TCGA) dataset. Among the 61 DElncRNAs, LINC00476 was identified as one of seven prognosis-associated lncRNAs (PAlncs) through a multivariable Cox proportional hazards regression analysis, with a $P < 0.01$[22] (Fig. 1A). Further, we found that the LINC00476 expression was decreased in many tumors from the TCGA/GTEx database (http://sangerbox.com/) (Fig. 1B). In PDAC, the lower expression of LINC00476 was significantly correlated with a more advanced stage (Fig. 1C). Similarly, the expression of LINC00476 was downregulated in tumor tissues in other public datasets (GSE16515, GSE15471, and

GSE28735) (Fig. 1D). The Kaplan–Meier survival analysis also revealed that a lower expression of LINC00476 was significantly correlated with poorer overall survival in PDAC (Fig. 1E).

We also confirmed that the expression of LINC00476 was downregulated in tumor tissue compared with uncancerous tissue through a micro-array of 60 pairs of PDAC by ISH (Table1 and Fig. 1F and G) There were no significant differences in LINC00476 expression in PDAC of different groups stratified by patient gender as well as their median age at diagnosis (Table 1). However, the higher expression of LINC00476 was correlated with early-stage [American joint committee on cancer (AJCC) stage I/II] negative lymph node metastasis and well differentiation of PDAC (Table 1). More importantly, the Kaplan–Meier analysis revealed that high LINC00476 expression was associated with better patient OS (Fig. 1H). Further multivariable Cox regression analysis revealed that high LINC00476 was a protective factor for prognosis in patients with PDAC of the GDPH cohort (Table 2). FISH staining revealed significantly reduced cytoplasmic LINC00476 expression in PDAC tissues compared with adjacent normal specimens (Fig. 1I). These results indicate that LINC00476 is downregulated in PDAC and might be a potential biomarker.

LINC00476 inhibits pancreatic cancer cell proliferation, invasion in vitro and inhibits tumor progression in vivo

To investigate the role of LINC00476 in PDAC, two PDAC cell lines (PANC-1 and MIA PaCa-2) were used for *in vitro* and *in vivo* functional assays. We performed qRT-PCR to determine the LINC00476 expression levels which was overexpressed using the dCAS9-SAM system (Fig. 2A) and knocked out by CRISPR-Cas9 in MIA PaCa-2 cells (Fig. 2B). We found that LINC00476 overexpression suppressed cell proliferation (Fig. 2C-F), cell mobility (Fig. 2G-H), and cell migration and invasion, as shown in *in vitro* functional assays (Fig. 2I and J), whereas enhanced in the LINC00476 knockout group.

To test the effect of LINC00476 *in vivo*, LINC00476 knockout PDAC cells and NC cells were inoculated into the right dorsal flanks of BALB/c nude mice. The mice injected with KO3 cells had higher tumor volume and tumor weight than those injected with Mia-NC cells (Fig. 2K and L). FISH and IHC staining confirmed the LINC00476 expression of xenograft tumors (Fig. 2M and N).These results indicate that LINC00476 inhibits pancreatic cancer cell proliferation, invasion both *in vitro* and *in vivo*.

An *in vivo* metastasis experiment was performed to validate the role of LINC00476 in PDAC metastasis. More metastatic tumor nodules and also higher tumor burden were observed in the livers of mice subjected to splenic injection of KO3 cells than control cells (Fig. 2O).

LINC00476 is localized in the cytoplasm and cytoskeleton, physically interacting with VIM

To explore the molecular mechanism by which LINC00476 affects pancreatic cancer progression, transcriptome sequencing was performed in LINC00476 overexpression cells. In total, 1738 DEGs (Log2|fold change| > 1.0 and adjusted *P*-value < 0.05) were obtained, and 699 DEGs were upregulated, whereas 1039 DEGs were downregulated (Supplemental Digital Content Figure S1A, available at: http://links.lww.com/JS9/F278; Supplemental Digital Content Table S4, available at: http://links.lww.com/JS9/F276). The KEGG analysis showed that LINC00476 and the DEGs were enriched in "Focal adhesion" and "Cell adhesion molecules" pathways (Fig. 3A). The function of lncRNAs is closely related to their sub-cellular localization. Thus, we next determined the subcellular localization of LINC00476. The GO analysis firstly indicated that LINC00476 was more likely to be localized in the cytoplasm (Supplemental Digital Content Figure S1B, available at: http://links.lww.com/JS9/F278). Then, similar to the FISH results in clinical samples (Fig. 1G), single-molecule RNA FISH in PANC-1, MIA PaCa-2, and AsPC-1 cells revealed that the LINC00476 molecules were localized in the cytoplasm and cytoskeleton (Fig. 3B). In addition, the nuclear and cytoplasmic separation assays further confirmed this finding (Supplemental Digital Content Figure S1C, available at: http://links.lww.com/JS9/F278). Based on its cytoplasmic localization, we suspected that LINC00476 might interact with cytoplasmic-specifc proteins. To identify the proteins associated with LINC00476, we transcribed biotinylated LINC00476 sense and antisense RNAs and performed RNA pull-down assays (Fig. 3C). The enriched proteins were separated using the sodium dodecyl sulfate–polyacrylamide gel electrophoresis (SDS–PAGE) for mass spectrometry and the results showed approximately 485 potentially interacting proteins (Supplemental Digital Content Table S5, available at: http://links.lww.com/JS9/F277). Subcellular localization enrichment analysis (GO-CC) indicated that most of the interacting proteins were localized in the cytoplasm and intermediate filament cytoskeleton (Fig. 3D). Indeed, VIM was identifed as a potential protein that bound to LINC00476. To validate the physical interaction between LINC00476 and VIM, we performed an RNA pull-down experiment and found that VIM was enriched in the RNA pull-down products in two PDAC cell lines transfected with LINC00476 (Fig. 3E). Moreover, RIP also showed the binding between them (Fig. 3F and G). Similarly, the results of the FISH and IF assays further confirmed the colocalization of LINC00476 and VIM (Fig. 3H). These findings suggest that LINC00476 physically interacts with VIM.

Next, a series of deletion mutants were constructed based on the secondary structure of LINC00476 (http://rna.tbi.univie.ac.at/cgi-bin/RNAWebSuite/RNAfold.cgi, Fig. 3I, Supplemental Digital Content Figure S2A-B, available at: http://links.lww.com/JS9/F278). We found that the deletion of the region containing nt 486-1270 impaired the binding between LINC00476 and VIM, indicating that this region mediated the interaction with VIM (Fig. 3J). Moreover, RIP assays with FLAG-tagged full-length and truncated VIM proteins showed that the deletion mutant lacking the binding domain (101-410 aa) of VIM failed to interact with LINC00476 (Fig. 3K, Supplemental Digital Content Figure S2C-D, available at: http://links.lww.com/JS9/F278). Thus, we identify the binding region of LINC00476 and the corresponding binding domain of VIM.

LINC00476 inhibits EMT by downregulating VIM in PDAC

We next investigated whether LINC00476 affected the expression level of VIM. We found that LINC00476 knockout or overexpression did not change the mRNA level of VIM (Fig. 4A). However, the protein level of VIM was dramatically decreased when LINC00476 was overexpressed and increased

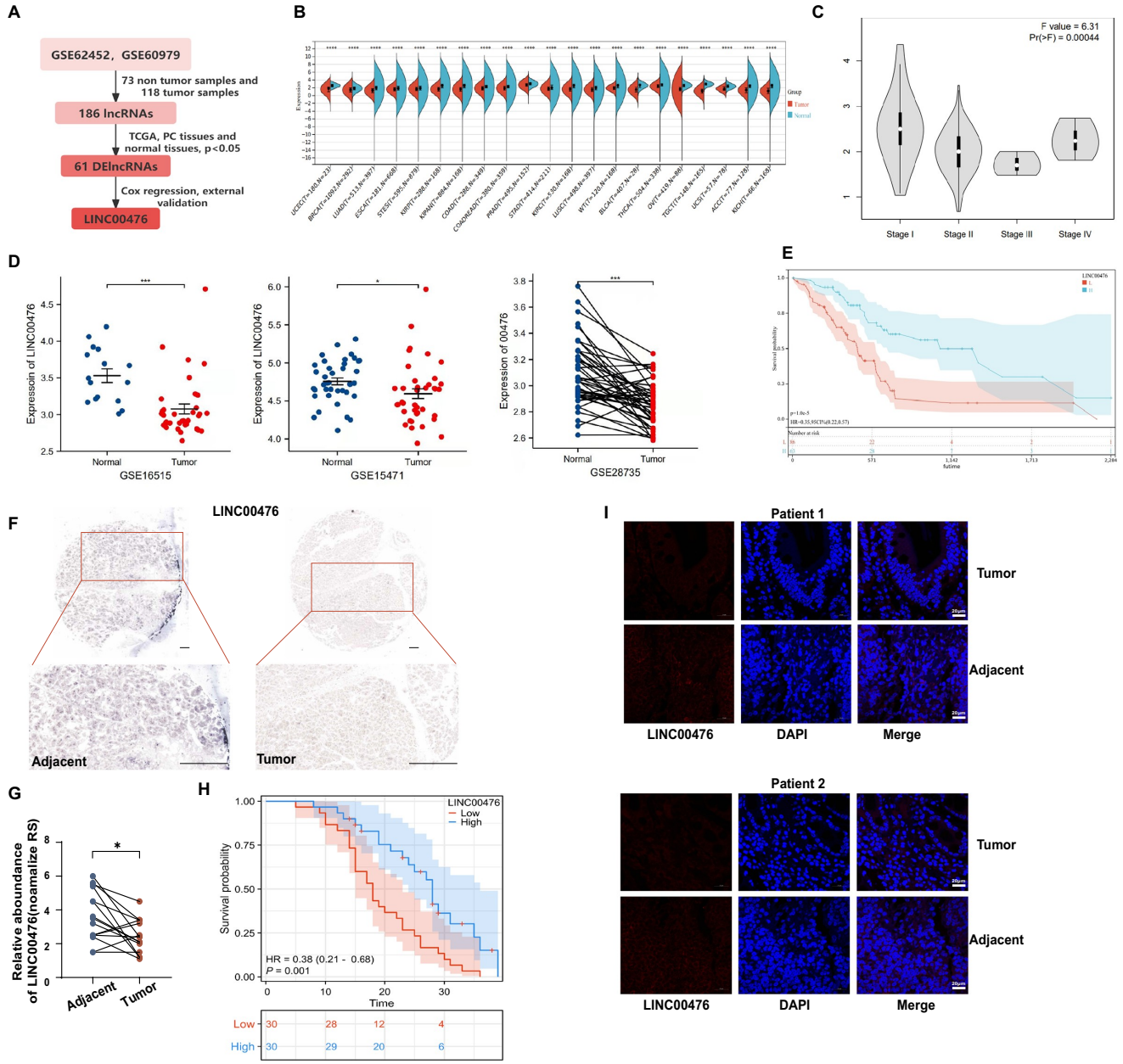

Figure 1. LINC00476 is downregulated in PDAC and associated with poor prognosis. (A) Flowchart showing the process used to identify DElncRNAs in patients with PDAC compared to that of healthy individuals from public datasets. (B) The expression of LINC00476 in multi-tumors from the TCGA+GTEx database. The non-parametric Mann–Whitney *U*-test. (C) The correlation between LINC00476 and pathological stage ($P = 0.00044$). Chi-square test or Fisher's exact tests. (D) The expression level of LINC00476 in GSE16515, GSE15471, and GSE28735 dataset. Two-tailed Student's *t*-test. (E) Kaplan–Meier survival curves for overall survival (OS) in the TCGA dataset in the high LINC00476 and low LINC00476 group ($P < 0.00001$). The log-rank test. Representative micrographs (F) and quantification (G) of LINC00476 expression in *in situ* hybridization (ISH) analysis in normal pancreatic tissue ($n = 30$) and PDAC tissue ($n = 30$). Scale bar = 100 μm; RS: risk score; Two-tailed Student's *t*-test. (H) Kaplan–Meier analysis of the probability of overall survival of PDAC patients in the hospital cohort. The log-rank test. (I) Representative images of FISH of LINC00476 (red) in PDAC and adjacent normal tissues. DAPI (blue) was used for nuclear counterstaining. *P* values are shown as $^{*}P < 0.05$, $^{***}P < 0.001$, $^{****}P < 0.0001$. All data represent the means ± SD from three independent assays.

when LINC00476 was knocked out (Fig. 4B). Taken together with the finding that LINC00476 binds to VIM protein, these findings indicate that LINC00476 may regulate VIM at the posttranslational level. In addition, we also found that the expression of other EMT-associated proteins were affected by LINC00476. Specifically, LINC00476 overexpression upregulated E-cadherin, an epithelial markers and downregulated N-cadherin and MMP9, which are mesenchymal markers. In contrast, LINC00476 knockout led to increased N-cadherin and MMP9 and decreased E-cadherin (Fig. 4C). These suggest that LINC00476 inhibits the EMT pathway in PDAC.

To further test whether the inhibitory effect of LINC00476 on pancreatic cancer progression is dependent on suppressing VIM, the LINC00476 overexpression PDAC cells were transfected with

Table 2

Univariate and multivariable Cox regression analysis of prognostic factors of outcome in 60 patients with PDAC

	Univariate analysis		Multivariate analysis	
Characteristics	**Hazard ratio (95% CI)**	***P* value**	**Hazard ratio (95% CI)**	***P* value**
LINC00476	0.382 (0.213–0.685)	**0.001**	0.384 (0.210–0.700)	**0.002**
Sex	0.820 (0.465–1.447)	0.493		
Age	0.775 (0.428–1.403)	0.400		
AJCC stage	1.834 (1.017–3.308)	**0.044**	1.411 (0.495–4.026)	0.519
Negative Lymph nodes	0.461 (0.249–0.854)	**0.014**	0.667 (0.222–2.009)	0.472
Differentiation	1.073 (0.608–1.893)	0.808		

AJCC, American Joint Committee on Cancer.

the VIM overexpressing plasmid for 48 h and the capacity of cell proliferation, migration, and invasion were evaluated. The results showed that VIM overexpressing partly or fully abrogated the inhibition effect of LINC00476 overexpression on cancer cell proliferation, migration, and invasion (Supplemental Digital Content Figure S3A-C, available at: http://links.lww.com/JS9/F278). These results imply that LINC00476 suppresses pancreatic cancer progression by targeting VIM.

LINC00476 facilitates VIM ubiquitination and degradation

Based on the above findings, we suspect that LINC00476 may affect the protein degradation of VIM. To test this hypothesis, we assessed the effect of LINC00476 on the turnover of VIM in PDAC cells after treatment with the protein synthesis inhibitor cycloheximide (CHX). The results showed that LINC00476 over-expression reduced the half-life of the VIM protein. Conversely, LINC00476 KO increased the half-life of the VIM protein, indicating that LINC00476 induces VIM degradation (Fig. 4D). The ubiquitin–proteasome system and lysosomal pathway are two types of regulators for intracellular proteolysis. We found that it was the proteasome inhibitor MG132, but not the autophagy inhibitor chloroquine (CQ), which abolishes lysosomal protein degradation leading to the accumulation of endogenous VIM in PDAC cells upon LINC00476 over-expression (Fig. 4E and F), suggesting that LINC00476 might induce VIM degradation via proteasome dependent pathway. Moreover, the ubiquitination levels of VIM were dramatically decreased in LINC00476-knocked out cells but increased in cells overexpressing LINC00476 (Fig. 4G). These suggest that LINC00476 facilitates VIM ubiquitination and degradation.

ARIH2 is necessary for LINC00476 induced VIM ubiquitination

lncRNAs have also been reported to act as scaffolds for protein complexes during processes that maintain cellular homeostasis, including protein ubiquitination[23,24]. Among the 485 potential LINC00476-interacting proteins detected by mass spectrometry, nine were previously reported E3 ubiquitinases ligases, namely PRPF19, RING1, RACK1, HUWE1, FAF2, CDC20, ARIH2, TRIM27, and FBXW11 (Fig. 5A). Interestingly, we found that the ARIH2 level was increased in LINC00476 overexpression cells (Fig. 5B). To test whether ARIH2 physically interacted with LINC00476, we performed ARIH2 RIP and LINC00476 pull-down assays and both assays showed the interaction between LINC00476 and ARIH2 (Fig. 5C and E). In addition, Co-IP and FISH assays showed that VIM also physically interacted and colocalized with ARIH2 and that this interaction was dependent on the presence of LINC00476 (Figs 5F and 6A). These results indicate that LINC00476, VIM, and ARIH2 form a specific complex, in which LINC00476 may serve as an assembly scaffold.

We next investigated the effect of ARIH2 on VIM ubiquitination. Ubiquitination assays revealed that VIM ubiquitination was positively regulated by ARIH2 expression (Fig. 6B and C). Moreover, following the treatment with CHX and MG132, ARIH2 overexpression reduced the half-life of the VIM protein whereas ARIH2 silencing had the opposite effect (Fig. 6D and E). These data suggest that ARIH2 is necessary for VIM ubiquitination and degradation. Prior evidence showed that RING2 contributes to the E3 ubiquitin ligase activity of the RBR motif, and a conserved cysteine in RING2 forms a transient thioester bond with ubiquitin, facilitating subsequent ubiquitin ligation to a lysine[24]. It has been reported that C300, which is located in the RING2 domain encoded by the amino acids 297–326 residues in ARIH2, plays a key role in the ubiquitination of NLRP3[24]. Based on this knowledge, we hypothesized that the RING2 domain of ARIH2 might interact with VIM to facilitate polyubiquitination (Supplemental Digital Content Figure S4A, available at: http://links.lww.com/JS9/F278). To test this, we generated an ARIH2 catalytically inactive mutant (C317A) and transfected it into PDAC cells. Consistent with our hypothesis, the C317A mutation abolished ARIH2-mediated VIM degradation, confirming that C317 was responsible for the enzyme activity of ARIH2 (Supplemental Digital Content Figure S4B and C, available at: http://links.lww.com/JS9/F278). It is important to note that the LINC00476 knockout still reduced the ubiquitination of VIM in PDAC cells even after ARIH2 overexpression (Fig. 6F). Collectively, these results indicate that LINC00476 acts as a molecular scaffold, facilitating the interaction of VIM with ARIH2, which decreases the stability of VIM by facilitating its ubiquitination-dependent degradation.

ARIH2 induces K29 ubiquitin-linked chain formation of VIM at Lys373

To clarify whether ARIH2-polyubiquitinated VIM is linked to any specific type of polyubiquitin chains, HEK-293T cells were

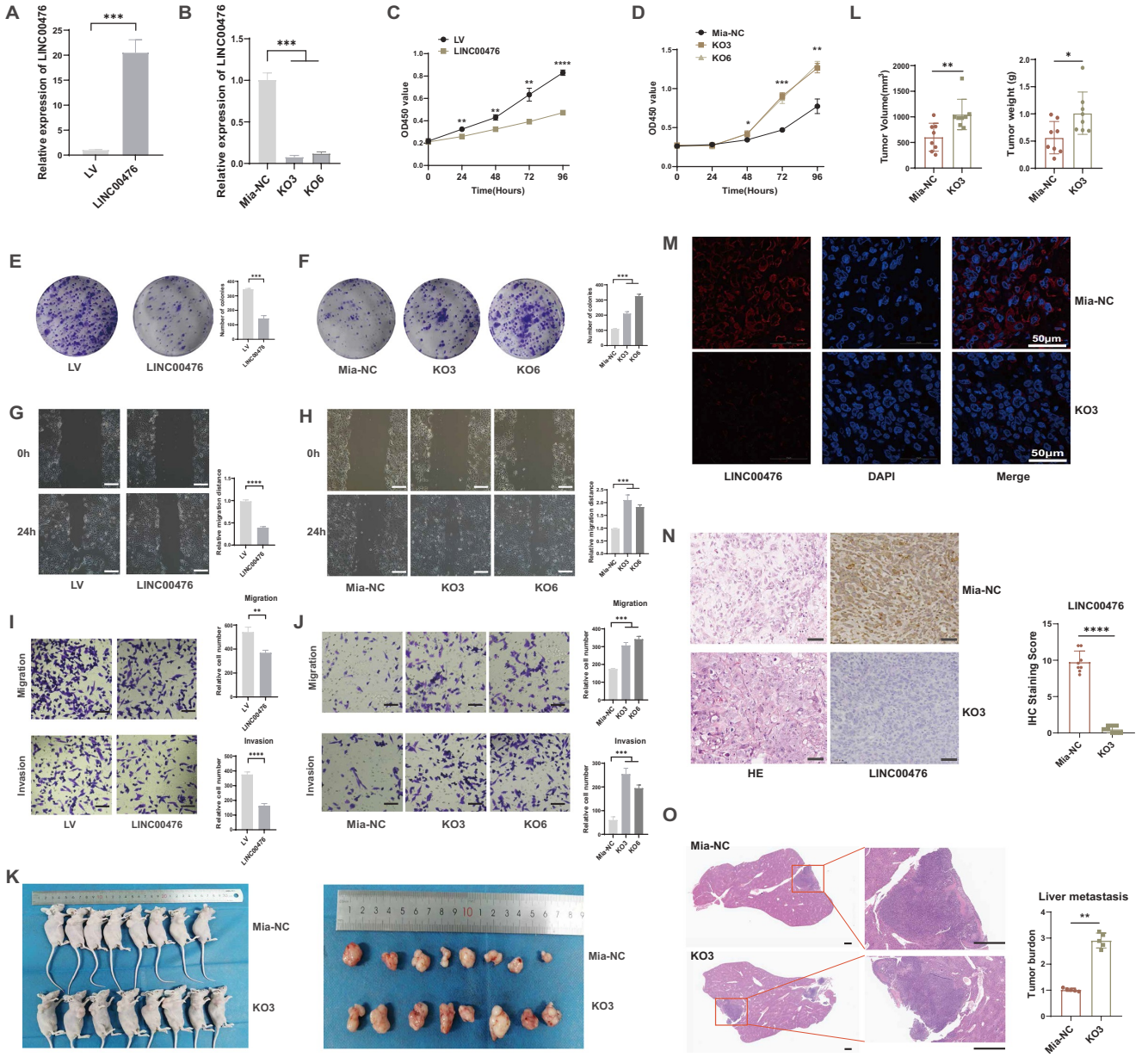

Figure 2. LINC00476 inhibits proliferation, invasion, and migration in PDAC. (A and B) The efficiency of LINC00476 overexpression in PANC-1 cells and LINC00476 knockout (KO3 and KO6) in MIA PaCa-2 cells were assessed using qRT-PCR. (C and D) CCK-8 assays were used to determine the cell proliferation rates in LINC00476 overexpression and LINC00476 knockout cells. (E and F) The effect of LINC00476 overexpression and knockout on colony formation was investigated in PDAC cell lines. (G and H) Representative images of wound healing assays after LINC00476 overexpression and knockout in PDAC cell lines. Scale bar = 100 μM. (I and J) Representative images of Migration and Invasion assays after LINC00476 overexpression and knockout in PDAC cell lines. Scale bar = 5 μM. (K) Representative images of subcutaneous tumors formed by the indicated cells. (L) Tumor weights and volume are expressed as the mean ± SD of eight mice. (M) Representative images of FISH of LINC00476 (red) in mice tissues. DAPI (blue) was used for nuclear counterstaining. (N) The representative images of H&E staining and ISH staining with LINC00476 probe in tumors. Scale bar = 50 μM. (O) Metastasis assays *in vivo* was performed by splenic injection to evaluate the efficiency of KO3 on tumor metastasis. Representative images of H&E staining in metastatic tumors formed by MIA PaCa-2 cells. Scale bar = 50 μM. *P* values are shown as $^{*}P < 0.05$; $^{**}P < 0.01$; $^{***}P < 0.001$; $^{****}P < 0.0001$. All *P*-values were assessed using two-tailed Student's *t*-test and one-way ANOVA followed by Tukey's multiple comparisons test. All data represent the means ± SD from three independent assays.

transiently transfected with Flag-VIM together with HA-Ub mutants (wild type, K27R, K29R, K48R, and K63R) in the presence or absence of His-ARIH2 treated with 10 μM MG132 for 6 h, and the VIM ubiquitination level in each condition were tested by Co-IP. We first found that the basic level of VIM ubiquitination, as well as the ARIH2-induced ubiquitination level of VIM, was significantly decreased in the presence of K27R and K29R but not in K48R or K63R mutants (Fig. 6G). Further experiments using the K27/K29-only ubiquitin mutants in which the lysine 27 and lysine 29 residue of ubiquitin was retained, whereas others were mutanted to arginine, revealed that ARIH2 specifically promoted a robust polyubiquitination of VIM by K29-only ubiquitin (HA-K29 Ub) in the same pattern as wild-type HA-Ub (Fig. 6H; Supplemental Digital Content

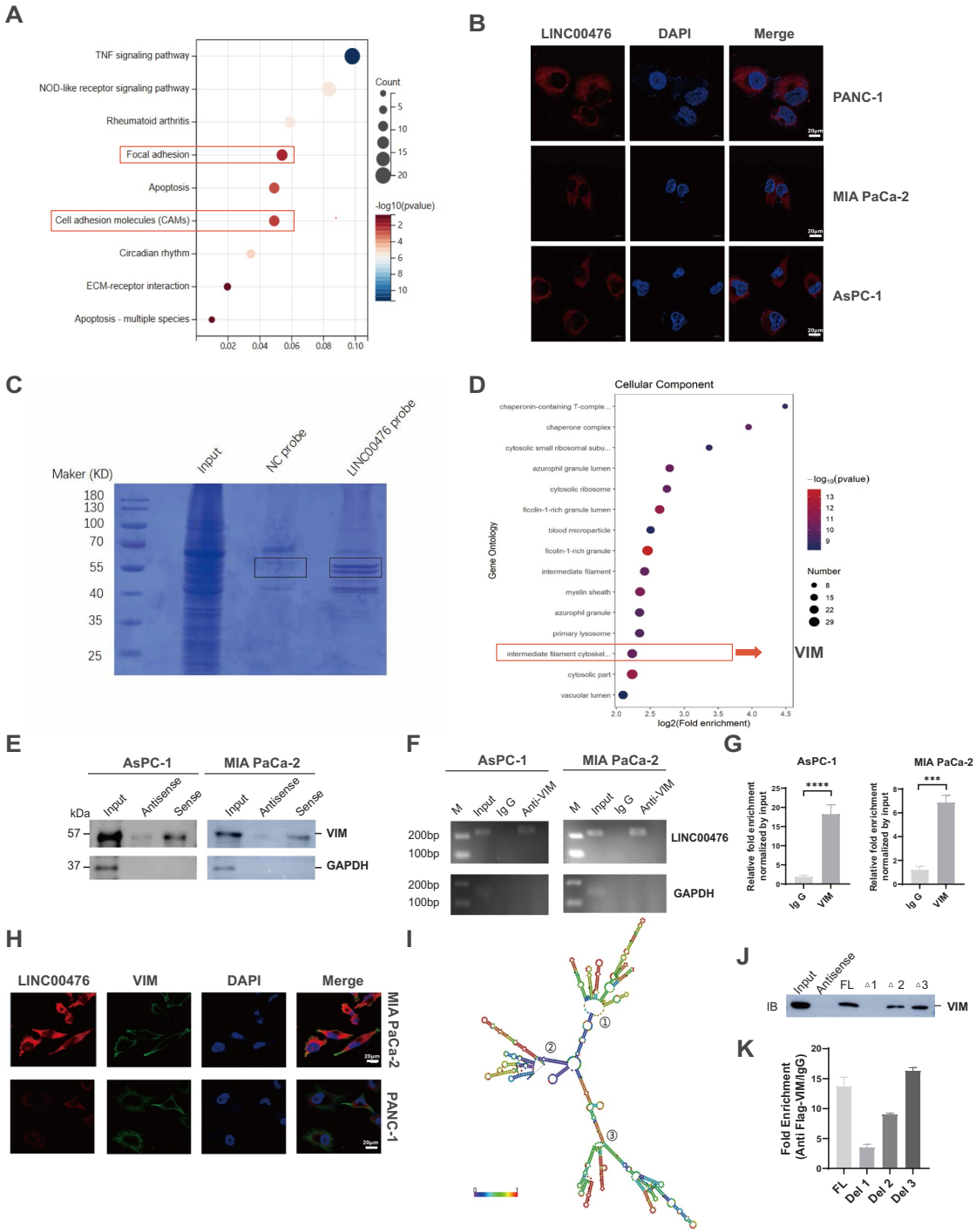

Figure 3. LINC00476 binds to VIM. (A) KEGG pathway analysis of LINC00476 based on transcriptome sequencing. (B) FISH staining showed that LINC00476 (red) was mainly localized in the cytoplasm and cytoskeleton. DAPI (blue) was used for nuclear counterstaining. (C) RNA pull-down assay was performed to detect the binding protein with biotinylated LINC00476. LINC00476 antisense RNA was used as the negative control. (D) GO-CC (cellular component) analysis predicting the potential proteins binding to LINC00476. (E) Western blotting was performed to evaluate the specific association of VIM with biotinylated LINC00476. Lysates of AsPC-1 and PANC-1 cells were harvested for RNA pull-down assays. LINC00476 antisense RNA was used as the negative control. (F and G) RNA-binding protein immunoprecipitation (RIP) assay was performed using an antibody against VIM. QRT-PCR was used to detect LINC00476 enrichment. IgG was used as the isotype control. Two-tailed Student's *t*-test. (H) FISH staining showed that LINC00476 (red) was colocalized with VIM (green). (I) Secondary structure of LINC00476 (http://www.Lncipedia.Org/). (J) Western blotting of VIM in samples precipitated by biotinylated full-length LINC00476 (FL) or LINC00476 truncations (Δ1: 1–485 bp; Δ2: 486–1024 bp; Δ3: 1025–1270bp). FL LINC00476 was used as the positive control. (K) Flag-RIP assay for LINC00476 showing its fold enrichment in cells transiently transfected with plasmids containing Flag-tagged full-length and truncated VIM constructs (Del1: 1–101 aa; Del2: 101–410 aa; Del3: 101–466 aa). IgG-RIP was used as the internal control. *P* values are shown as ***$P < 0.001$; ****$P < 0.0001$. All data represent the means ± SD from three independent assays.

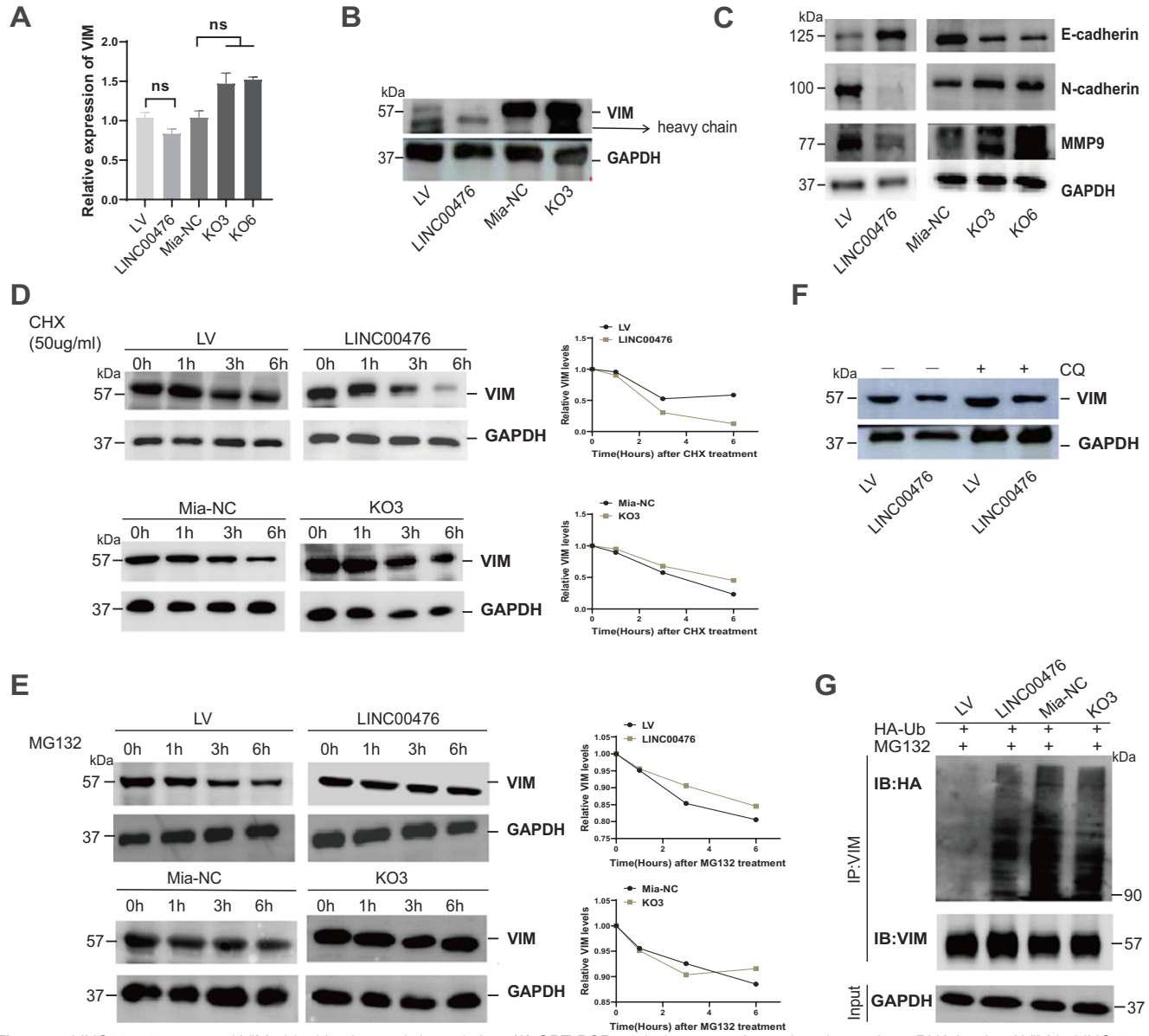

Figure 4. LINC00476 promoted VIM ubiquitination and degradation. (A) QRT-PCR analysis was performed to detect the mRNA levels of VIM in LINC00476 overexpression and knockout cells. Two-tailed Student's *t*-test and one-way ANOVA followed by Tukey's multiple comparisons test. (B and C) The protein levels of E-cadherin, N-cadherin, MMP9, and VIM in LINC00476 overexpression and knockout cells. GAPDH was used as the internal control. (D) The protein levels of VIM in the indicated cells treated with cycloheximide (CHX, 50 μg/mL) for 0, 1, 3, and 6 h. (E) The protein levels of VIM in the indicated cells treated with MG132 (10 μM) for 0, 1, 3, and 6 h. (F) The protein levels of VIM in the indicated cells treated with or without chloroquine (CQ, 10 μM) for 6 h. (G) The ubiquitination levels of VIM were determined by Western blotting. LINC00476 overexpression and knockout cells treated with MG132 for 4 h before cell lysates were harvested for coimmunoprecipitation with an anti-VIM antibody and immunoblotted with an anti-HA antibody. All the experiments were performed in triplicates.

Figure S5A, available at: http://links.lww.com/JS9/F278). Taken together, these results indicate that the poly ubiquitination of VIM by ARIH2 may be dependent on K29 ubiquitin-linked chain formation.

Based on the fact that ubiquitination occurs at lysine residues of target proteins, we analyzed the amino acid sequence of VIM and found only one lysine residue in the body domain of VIM (Fig. 3K, Supplemental Digital Content Figure S2C and D, available at: http://links.lww.com/JS9/F278). To examine whether this residue is responsible for the ARIH2-mediated polyubiquitination of VIM, we generated a VIM mutant (K373A) by replacing Lys373, which is evolutionarily conserved in different species, with alanine (Supplemental Digital Content Figure S5B, available at: http://links.lww.com/JS9/F278). Indeed, we found that though wild-type VIM was subjected to polyubiquitination by ARIH2, the VIM (K373A) mutant did not undergo polyubiquitination (Supplemental Digital Content Figure S5C, available at: http://links.lww.com/JS9/F278). Additionally, cycloheximide treatment revealed that the stability of the VIM (K373A) mutant was not influenced by ARIH2 (Supplemental Digital Content Figure S5D, available at: http://links.lww.com/JS9/F278). Thus, the Lys373 residue of VIM is a major target of ARIH2-induced

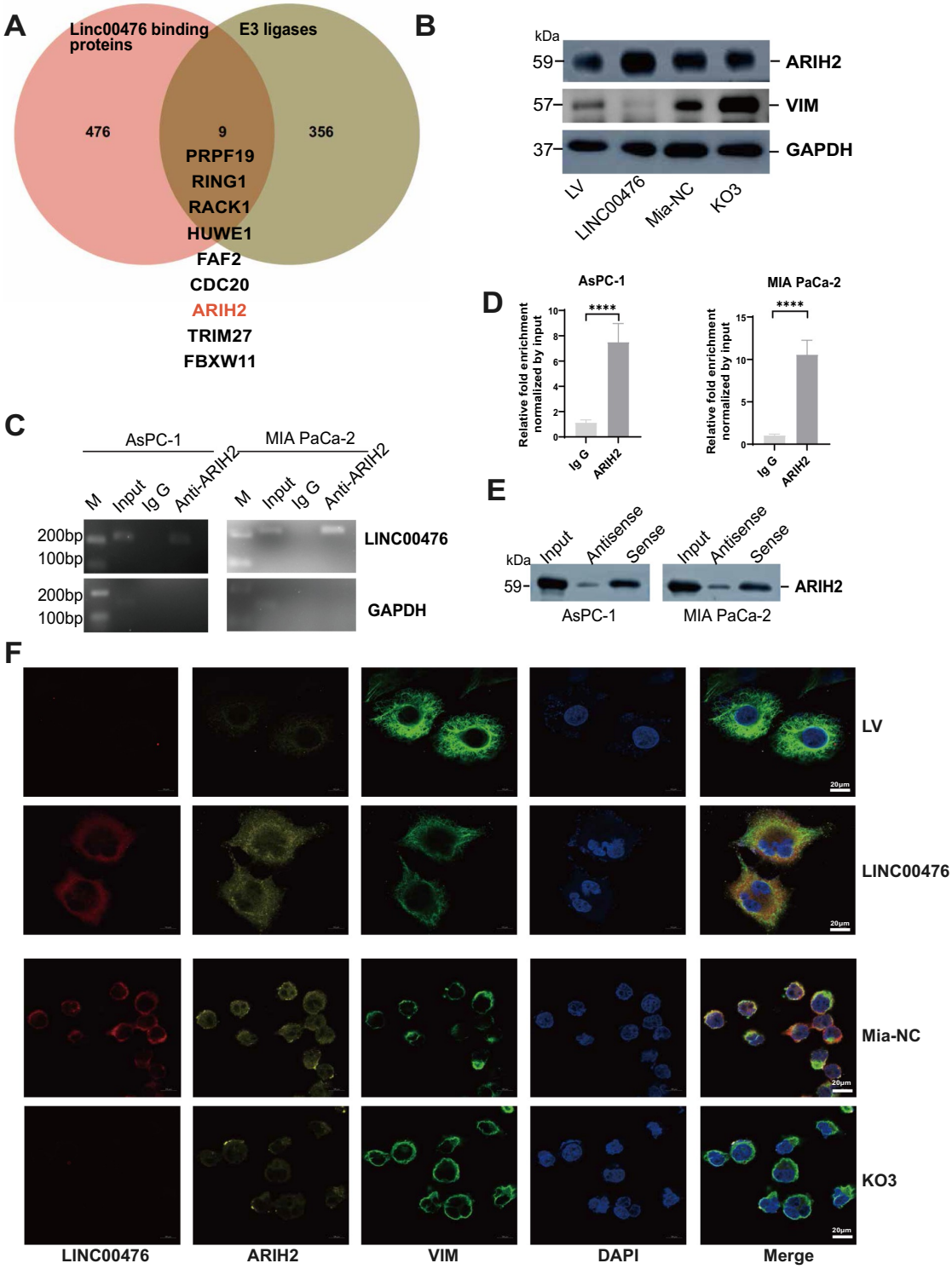

Figure 5. ARIH2 is the E3 ligases for VIM. (A) Venn diagram for identifying nine candidate E3 ligases overlapping with the potential binding proteins of LINC00476. (B) The protein level of ARIH2 in LINC00476 overexpression and knockout cells. (C and D) A RNA-binding protein immunoprecipitation (RIP) assay was performed using an antibody against VIM. QRT-PCR was used to detect LINC00476 and VIM enrichment. IgG was used as the isotype control. Two-tailed Student's *t*-test. (E) Western blotting was performed to evaluate the specific association of ARIH2 with biotinylated LINC00476. Lysates of AsPC-1 and MIA PaCa-2 cells were harvested for RNA pull-down assays. LINC00476 antisense RNA was used as the negative control. (F) FISH staining showed that LINC00476 (red) was colocalized with ARIH2 (yellow) and VIM (green) in the LINC00476 overexpression and knockout cells. DAPI (blue) was used for nuclear counterstaining. *P* values are shown as ****$P < 0.0001$. All data represent the means ± SD from three independent assays.

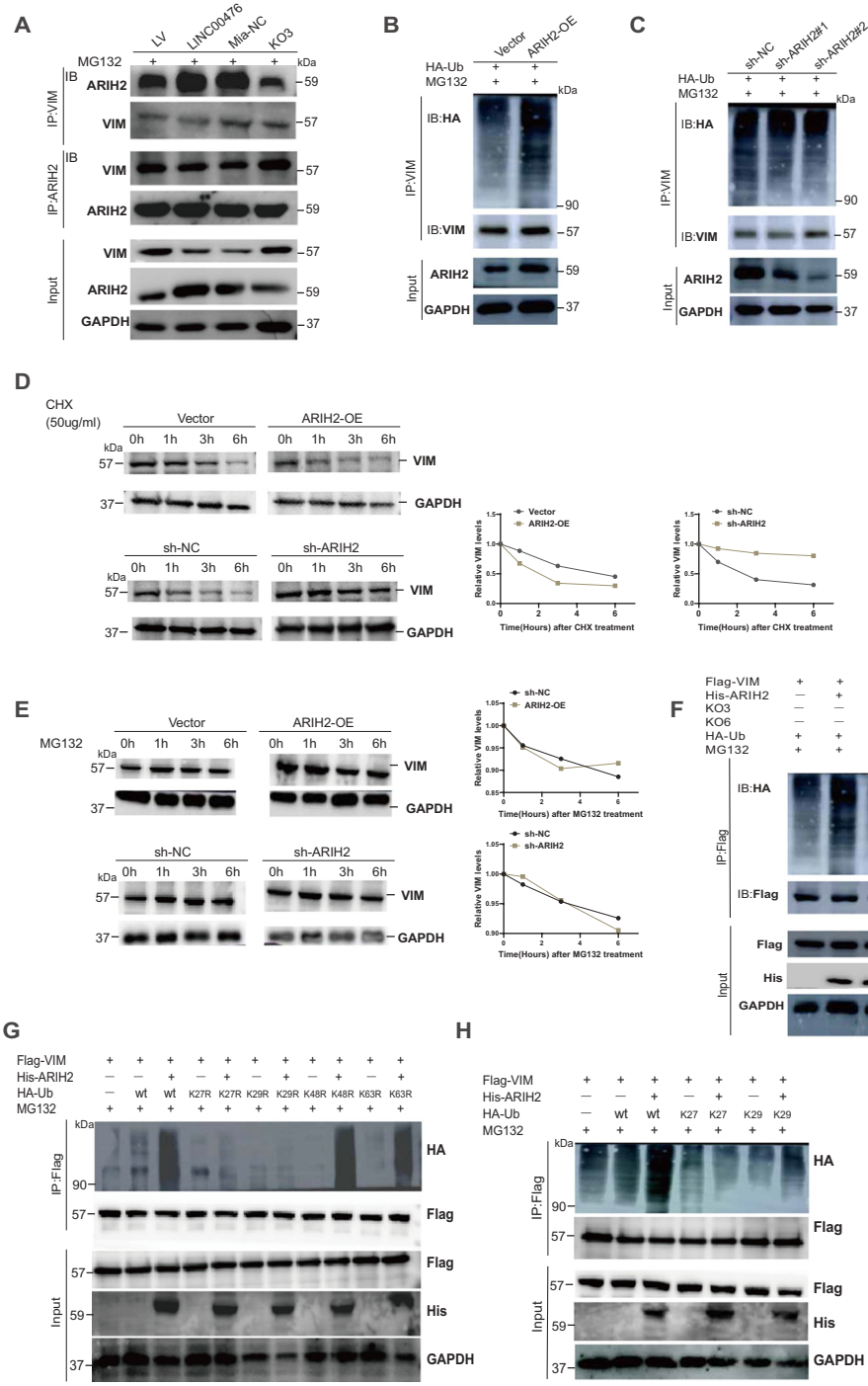

Figure 6. ARIH2 is necessary for LINC00476 induced VIM ubiquitination. (A) The protein levels of VIM and ARIH2 were determined by Western blotting. LINC00476 overexpression and KO3 cells treated with MG132 for 4 h before cell lysates were harvested for co-IP with an anti-VIM antibody and anti-ARIH2 antibody. (B and C) The ubiquitination levels of VIM were determined by Western blotting. AsPC-1 cells were transiently transfected with ARIH2 overexpression (B), MIA PaCa-2 cells transfected ARIH2 silencing (C) and also with the corresponding control plasmids and then treated with MG132 for 4 h before cell lysates were harvested for co-IP with an anti-VIM antibody and immunoblotted with an anti-HA antibody. (D) The protein levels of ARIH2 in MIA PaCa-2 and AsPC-1 cells treated with cycloheximide (CHX, 50 μg/mL) for 0, 1, 3, and 6 h. AsPC-1 cells transfected with ARIH2 overexpression (upper), MIA PaCa-2 cells transfected with ARIH2 silencing (lower). (E) The protein levels of ARIH2 in MIA PaCa-2 and AsPC-1 cells treated with MG132 (10 μM) for 0, 1, 3, and 6 h. AsPC-1 cells transfected with ARIH2 overexpression (upper), MIA PaCa-2 cells transfected with ARIH2 silencing (lower). (F) The ubiquitination levels of VIM in the products of IP with an anti-Flag antibody in lysates from LINC00476 knockout or ARIH2 overexpression and control plasmids. (G) Immunoprecipitation assay showing K29-mediated ubiquitination of VIM by ARIH2. The 293T cells were cotransfected with Flag-VIM, different linkages of HA-ubiquitin mutant (wild-type, K27R, K29R, K49R, and K63R), or His-ARIH2 plasmids; and then, cell lysates were immunoprecipitated with anti-Flag antibody. (H) Flag-VIM plasmid was cotransfected into 293T cells together with wild-type, K27, K29, or lysine mutant (K27R and K29R) of HA-Ubiquitin in the absence or presence of His-ARIH2 plasmid. Cell lysates were immunoprecipitated with anti-Flag antibody and then immunoblotted with the indicated antibodies. All data represent the means ± SD from three independent assays.

polyubiquitination, which regulates VIM stability. Taken together, our results suggest that ARIH2 induces the K29 ubiquitin-linked chain formation of VIM at Lys373 in PDAC cells.

ARIH2 inhibits pancreatic cancer cell proliferation, invasion in vitro and suppresses tumor growth in a PDX model

Our findings led us to verify the physiological function of LINC00476 in pancreatic cancer progression and ARIH2 was necessary for LINC00476-mediated VIM ubiquitination. We then investigated whether the expression level of ARIH2 affects tumorigenesis *in vitro* and *in vivo*. Knockdown of VIM reduced the aggressive potential, whereas simultaneous knockdown of ARIH2 may be sufficient to rescue an aggressive phenotype and cancer progression in MIA PaCa-2 cells (Supplemental Digital Content Figure S6A and B, available at: http://links.lww.com/JS9/F278; Supplemental Digital Content Figure S7A–C, available at: http://links.lww.com/JS9/F278). Similarly, ARIH2 overexpression markedly decreased the proliferation, migration and invasion of AsPC-1 cells, whereas VIM overexpression reversed the suppressive effects of ARIH2 (Supplemental Digital Content Figure S6A and B, available at: http://links.lww.com/JS9/F278; Supplemental Digital Content Figure S8A–C, available at: http://links.lww.com/JS9/F278).

Finally, we investigated the role of ARIH2 in regulating VIM and tumor growth *in vivo* by employing a PDX model in mice. In brief, ARIH2 overexpression virus and vector virus were administered to the PDX bearing mice via intratumoral injection (Fig. 7A). We found that ARIH2 overexpression significantly decreased the tumor burden compared to control group (Fig. 7B–E). Importanly, ARIH2 over-expression led to decreased VIM and increased E-cadherin, decreased N-cadherin, indicating that ARIH2 inhibits VIM and EMT *in vivo* (Fig. 7F). In addition, ARIH2 overexpression surprisingly suppressed the LINC00476 expression (Fig. 7G). Thus, ARIH2 inhibits pancreatic cancer progression by decreasing VIM.

Discussion

lncRNAs play a very important role in regulating tumorigenicity and tumor progression and they may be effective biomarkers for cancer detection and diagnosis. In our study, we identified a novel lncRNA, LINC00476, as a favorable biomarker for PDAC. By using bioinformatic analysis based on public datasets, we found that LINC00476 was downregulated in PDAC and lower expression of LINC00476 was related to poorer clinicopathological features and patients survival. Importantly, LINC00476 was found to negatively regulate VIM and EMT in both PDAC cells and mice model, indicating that it may act as a tumor suppressor in PDAC.

VIM expression is a hallmark of EMT, which is characterized by epithelial cells losing cell-and-cell contacts and gain a fibroblast-like morphology and is a critical early step for cancer metastasis. The dysregulation of VIM including PTM for VIM is reported in malignant cancers, which promotes cancer progression and metastasis[25,26]. In our study, we found that VIM ubiquitination was decreased in PDAC, leading to VIM stabilization and enhanced EMT phenotype. Specifically, VIM ubiquitination was regulated by LINC00476 and ARIH2. Other studies also demonstrated VIM ubiquitination, affected by distinct proteins or LncRNAs[13,27,28]. In ovarian cancer cells, Trim56 was found to be the ubiquitin ligase for VIM[18], and Trim16 was the E3 ligase responsible for VIM ubiquitination in LAD cells[28]. These indicate that protein ubiquitination is a critical way for regulating VIM degradation and there is heterogeneity for VIM ubiquitin ligase among different cancers. Importantly, we identified that the Lys373 residue was the ubiquitination site for VIM, which was also specific in PDAC. It will be of much interest to design a treating strategy to induce VIM ubiquitination and degradation by targeting Lys373 residue in PDAC in the future studies.

Ubiquitination is a key determinant of protein degradation. Recently, lncRNAs have been found to modulate PTM including protein ubiquitination in cancers[29,30]. Normally, lncRNAs may interact with proteins and prevent the PTM by masking sites bound by PTM enzymes or PTM sites. For example, Zhang *et al* found that LncRNA BREA2 bound to NICD1 and prevented the physical interaction between NICD1 and WWP2, a E3 ubiquitin ligase, leading to the inhibition of NICD1 ubiquitination[31]. However, in our study, LINC00476 promoted VIM ubiquitination in PDAC by acting as a scaffold, which supported the interaction of VIM with ARIH2. Other ubiquitination associated lncRNAs were also reported. Zhang *et al* showed that lncRNA HEPFAL also promoted the ubiquitination of SLC7A11 and reduced the stability of the SLC7A11 protein, although they did not provide detailed mechanism like the ubiquitin ligase or ubiquitin site[32]. Taken together, lncRNAs may promote or prevent protein ubiquitination in distinct circumstances. Future studies are needed to figure out the effect of the binding site or binding structure between lncRNA and the corresponding proteins on the ubiquitination regulation.

ARIH2 is a member of the Ariadne subfamily ligase of the RBR E3 ligase and it contains two RING fingers and a double RING finger linked 1 (Triad1) protein with E3 ubiquitin ligase activity[33]. RBR E3 ligases have diverse functions in human cancers[34]. Among them, RNF14, RNF31, RNF144B, RNF216, and ARIH1 were reported to mainly play carcinogenic roles, whereas ARIH2 and PARK2 may have anticancer effect[35,36]. In a study, it was found that ARIH2 promoted Nutlin-3a-triggered p53 activation and led to cell death in multiple cancer cells, including MCF7, U2OS, and A549 cells[32]. Moreover, the knockdown of ARIH2 is involved in resistance to epidermal growth factor receptor tyrosine kinase inhibitors in human non-small cell lung cancer[37]. However, Geng *et al*[38] showed the opposite effect of ARIH2 in gastric cancer. They found that ARIH2 promoted gastric cancer cell proliferation by regulating p21 ubiquitination. In our study, we discovered that ARIH2 inhibits the proliferation of PDAC cells and may also play an anticancer role. Our studies showed that ARIH2 regulated VIM via ubiquitination, which was dependent on LINC00476 (Fig. 7H). It will be interesting to determine whether lncRNA dependency is a general mechanism for ARIH2 induced ubiquitination in future studies.

Conclusion

In conclusion, we demonstrate that LINC00476 downregulates VIM and inhibits the EMT process, thereby suppressing tumor progression. In particular, LINC00476 cooperates with ARIH2 and induces VIM ubiquitination. Our study indicates that

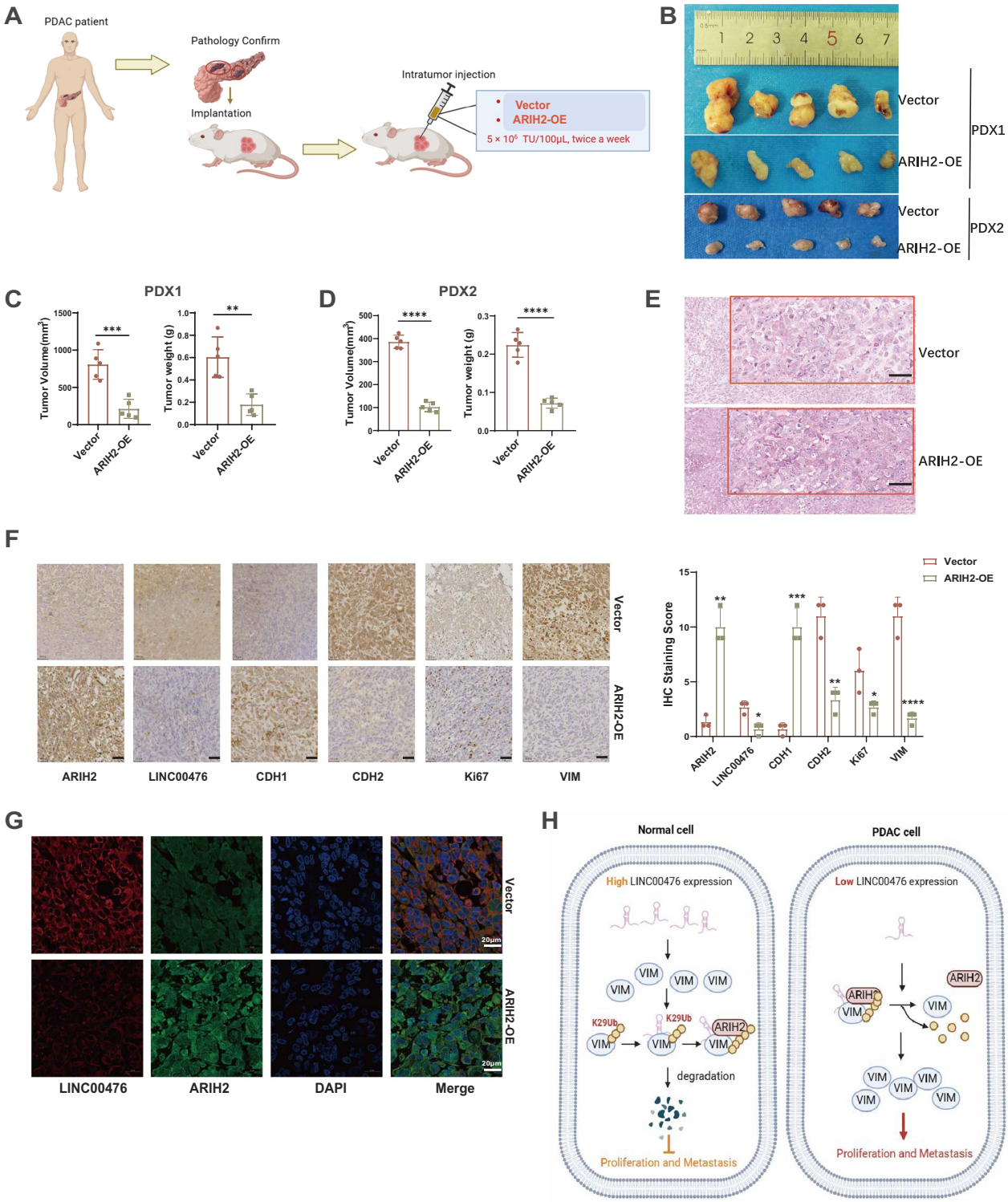

Figure 7. ARIH2 decreases VIM and suppresses tumor growth in a PDX model. (A) Graphical diagram of intratumoral injection of *in vivo* optimized ARIH2 overexpression and control lentivirus in PDX-bearing mice. (B) Representative images of xenograft tumors derived from PDX in each mouse group. Mice bearing xenograft tumors were treated with ARIH2 overexpression (ARIH2-OE) and control (Vector) lentivirus. (C and D) Xenograft tumor growth was monitored by measuring the tumor volume and weighing the tumors. Tumor volume and weight are expressed as the mean ± SD of five mice. Two-tailed Student's *t*-tests. (E and F) Representative images of H&E staining, ISH staining of LINC00476 and IHC staining of CDH1, CDH2, Ki67, and VIM of xenograft tumors. Scale bar = 50 μM. Two-tailed *t*-tests. (G) Representative images of FISH and IF staining showed that the expression of LINC00476 (red) was lower compared to ARIH2 (green) overexpression in PDX models. DAPI (blue) was used for nuclear counterstaining. (H) Schematic diagram of the effect of the LINC006476/VIM axis on the tumorigenicity and progression and metastasis of PDAC. *P* values are shown as**P* <0.05; ***P* < 0.01; ****P* < 0.001; *****P* < 0.0001. All data represent the means ± SD from three independent assays.

LINC00476 is a tumor suppressor and biomarker for PDAC, which deserves further investigation.

Ethical approval

The Ethics Committee of Guangdong Provincial Hospital affiliated with Southern Medical University approved the study on 2 August 2021 (KY-Z-2020-169-2).

Consent

Written informed consent was obtained from the patient for the publication of this case report and accompanying images. A copy of the written consent is available for review by the Editor-in-Chief of this journal on request.

Sources of funding

This work was supported by grants from the National Natural Science Foundation of China (82472762), High-level Hospital Construction Research Project of Heyuan People's Hospital (YNKT202202), Guangdong Province's Special Fund for Science and Technology Innovation Strategy ("Major Project + Task List") Project of Heyuan (230510171473335/2022001), the Science and Technology Program of Guangzhou (2024A04J10016), Young Talent Support Project of Guangzhou Association for Science and Technology (QT2024-037), Guangdong Basic and Applied Basic Research Funding, Guangdong Province (2025A1515012422).

Author contributions

Q.Y., B.H., C.Z., and S.H. contributed to the conception. Q.Y., Y.C., and Z.L. analyzed the data and formal analysis; C.Z., S. H., and B.H. contributed to the funding acquisition. Q.Y., C.Z., and S.H. drafted the original manuscript; Q.Y., Y.C., L.Z., C.Z., S.H., and B.H. polished and revised the manuscript. This manuscript has been read and approved by all authors.

Conflicts of interest disclosure

The authors declare that they have no competing interests.

Guarantor

Baohua Hou.

Research registration unique identifying number (UIN)

Not applicable.

Provenance and peer review

Not commissioned, externally peer-reviewed.

Data availability statement

The datasets used and/or analyzed during the current study are available from the corresponding author on reasonable request.

References

[1] Siegel RL, Giaquinto AN, Jemal A. Cancer statistics, 2024. CA Cancer J Clin 2024;74:12–49.
[2] Kuehn BM. Looking to long-term survivors for improved pancreatic cancer treatment. Jama 2020;324:2242–44.
[3] Mizrahi JD, Surana R, Valle JW, Shroff RT. Pancreatic cancer. Lancet 2020;395:2008–20.
[4] Quinn JJ, Chang HY. Unique features of long non-coding RNA biogenesis and function. Nat Rev Genet 2016;17:47–62.
[5] Huarte M. The emerging role of lncRNAs in cancer. Nat Med 2015;21:1253–61.
[6] Zhang H, Wei P, Lv W, Han X, Yang J, Qin S. Long noncoding rna lnc-dilc stabilizes pten and suppresses clear cell renal cell carcinoma progression. Cell Biosci 2019;9:81.
[7] Qiao Y, Jin T, Guan S, *et al*. Long non-coding RNA lnc-408 promotes invasion and metastasis of breast cancer cell by regulating limk1. Oncogene 2021;40:4198–213.
[8] Tian Y, Ai M, Liu C, *et al*. Upregulated long non-coding RNA lnc-mrpl39-2:1 induces the growth and invasion of nasopharyngeal carcinoma by binding to HuR and stabilizing beta-catenin mRNA. Int J Biol Sci 2023;19:2349–65.
[9] Li Z, Ma Z, Wang S, *et al*. Linc00909 up-regulates pluripotency factors and promotes cancer stemness and metastasis in pancreatic ductal adenocarcinoma by targeting smad4. Biol Direct 2024;19:24.
[10] Yang Q, Li K, Huang X, *et al*. Lncrna slc7a11-as1 promotes chemoresistance by blocking scf(beta-trcp)-mediated degradation of nrf2 in pancreatic cancer. Mol Ther Nucleic Acids 2020;19:974–85.
[11] Li H, Wang X, Wen C, *et al*. Long noncoding rna norad, a novel competing endogenous rna, enhances the hypoxia-induced epithelial-mesenchymal transition to promote metastasis in pancreatic cancer. Mol Cancer 2017;16:169.
[12] Parvanian S, Coelho-Rato LS, Patteson AE, Eriksson JE. Vimentin takes a hike - emerging roles of extracellular vimentin in cancer and wound healing. Curr Opin Cell Biol 2023;85:102246.
[13] Feng H, Xu D, Jiang C, *et al*. Linc01559 promotes lung adenocarcinoma metastasis by disrupting the ubiquitination of vimentin. Biomark Res 2024;12:19.
[14] Zhu Z, Rong Z, Luo Z, *et al*. Circular rna circnhsl1 promotes gastric cancer progression through the mir-1306-3p/six1/vimentin axis. Mol Cancer 2019;18:126.
[15] Dey R, Burkhard P. A proposed atomic model of the head-to-tail interaction in the filament structure of vimentin. J Biomol Struct Dyn 2020;38:4921–27.
[16] Snider NT, Omary MB. Post-translational modifications of intermediate filament proteins: mechanisms and functions. Nat Rev Mol Cell Biol 2014;15:163–77.
[17] Kraxner J, Lorenz C, Menzel J, *et al*. Post-translational modifications soften vimentin intermediate filaments. Nanoscale 2021;13:380–87.
[18] Zhao L, Zhang P, Su XJ, Zhang B. The ubiquitin ligase trim56 inhibits ovarian cancer progression by targeting vimentin. J Cell Physiol 2018;233:2420–25.
[19] Cui G, Fu X, Wang W, *et al*. Linc00476 suppresses the progression of non-small cell lung cancer by inducing the ubiquitination of setdb1. Radiat Res 2021;195:275–83.
[20] Kilkenny C, Browne WJ, Cuthill IC, Emerson M, Altman DG. Improving bioscience research reporting: the ARRIVE guidelines for reporting animal research. PLoS Biol 2010;8:e1000412.
[21] Liu J, Liu ZX, Wu QN, *et al*. Long noncoding rna agpg regulates pfkfb3-mediated tumor glycolytic reprogramming. Nat Commun 2020;11:1507.
[22] Zhuang H, Huang S, Zhou Z, *et al*. A four prognosis-associated lncRNAs (palnc) based risk score system reflects immune cell infiltration and predicts patient survival in pancreatic cancer. Cancer Cell Int 2020;20:493.
[23] Zhang C, Ge S, Gong W, *et al*. Lncrna anril acts as a modular scaffold of wdr5 and hdac3 complexes and promotes alteration of the vascular smooth muscle cell phenotype. Cell Death Dis 2020;11:435.
[24] Zhao P, Ji MM, Fang Y, *et al*. A novel lncrna tcllnc1 promotes peripheral t cell lymphoma progression through acting as a modular scaffold of hnrnpd and ybx1 complexes. Cell Death Dis 2021;12:321.
[25] Chang WH, Chen YJ, Hsiao YJ, *et al*. Reduced symmetric dimethylation stabilizes vimentin and promotes metastasis in MTAP-deficient lung cancer. EMBO Rep 2022;23:e54265.

[26] Dong Z, Min F, Zhang S, Zhang H, Zeng T. Egr1-driven mettl3 activation curtails vim-mediated neuron injury in epilepsy. Neurochem Res 2023;48:3349–62.
[27] Shao W, Li J, Piao Q, *et al*. Frmd3 inhibits the growth and metastasis of breast cancer through the ubiquitination-mediated degradation of vimentin and subsequent impairment of focal adhesion. Cell Death Dis 2023;14:13.
[28] Jiang Y, Feng Y, Huang J, *et al*. Lad1 promotes malignant progression by diminishing ubiquitin-dependent degradation of vimentin in gastric cancer. J Transl Med 2023;21:632.
[29] Zhao W, Zhang D, Qin P, *et al*. Long non-coding RNA epic1 inhibits viability and invasion of osteosarcoma cells by promoting mef2d ubiquitylation. Int J Biol Macromol 2019;128:566–73.
[30] Tsang SV, Rainusso N, Liu M, *et al*. Lncrna pvt-1 promotes osteosarcoma cancer stem-like properties through direct interaction with trim28 and tsc2 ubiquitination. Oncogene 2022;41:5373–84.
[31] Zhang Z, Lu YX, Liu F, *et al*. Lncrna brea2 promotes metastasis by disrupting the wwp2-mediated ubiquitination of notch1. Proc Natl Acad Sci U S A 2023;120:e2088273176.
[32] Zhang B, Bao W, Zhang S, *et al*. Lncrna hepfal accelerates ferroptosis in hepatocellular carcinoma by regulating slc7a11 ubiquitination. Cell Death Dis 2022;13:734.
[33] Wu C, Zhang H, Hong H, *et al*. E3 ubiquitin ligase triad1 promotes neuronal apoptosis by regulating the p53-caspase3 pathway after spinal cord injury. Somatosens Mot Res 2022;39:21–28.
[34] Wang P, Dai X, Jiang W, Li Y, Wei W. Rbr e3 ubiquitin ligases in tumorigenesis. Semin Cancer Biol 2020;67:131–44.
[35] Dove KK, Klevit RE. Ring-between-ring e3 ligases: emerging themes amid the variations. J Mol Biol 2017;429:3363–75.
[36] Walden H, Rittinger K. Rbr ligase-mediated ubiquitin transfer: a tale with many twists and turns. Nat Struct Mol Biol 2018;25:440–45.
[37] Zeng H, Castillo-Cabrera J, Manser M, *et al*. Genome-wide CRISPR screening reveals genetic modifiers of mutant EGFR dependence in human NSCLC. Elife 2019;8:e50223.
[38] Geng S, Peng W, Wang X, *et al*. Arih2 regulates the proliferation, dna damage and chemosensitivity of gastric cancer cells by reducing the stability of p21 via ubiquitination. Cell Death Dis 2022;13:564.